applied sciences

MDPI

Article

Temperature-Dependent Mitigation of Sodium Lignosulfonate Adsorption on Buff Berea Sandstone Using Silica Nanoparticles for Chemical Enhanced Oil Recovery

Sarah Dampang [1], Putri Masruroh [2], Selly Arvinda Rakhman [3], Azafilmi Hakiim [1], Hasti Asfarina [3], Farradina Choria Suci [3], Setyo Budi Kurniawan [4] and Muhammad Fauzul Imron [5,6,7,*]

1 Study Program of Chemical Engineering, Faculty of Engineering, Universitas Singaperbangsa Karawang, Karawang 41361, Indonesia; sarah.dampang@staff.unsika.ac.id (S.D.); azafilmi.hakiim@staff.unsika.ac.id (A.H.)
2 Diploma Program in Mechanical Engineering, Faculty of Engineering, Universitas Singaperbangsa Karawang, Karawang 41361, Indonesia; putri.masruroh@ft.unsika.ac.id
3 Study Program of Chemistry, Faculty of Engineering, Universitas Singaperbangsa Karawang, Karawang 41361, Indonesia; selly.arvinda@ft.unsika.ac.id (S.A.R.); hasti.asfarina@ft.unsika.ac.id (H.A.); farradina.cs@ft.unsika.ac.id (F.C.S.)
4 Research Center for Environment and Clean Technologies, National Research and Innovation Agency (BRIN), Jakarta Pusat 10340, Indonesia; setyo.budi.kurniawan@brin.go.id
5 Study Program of Environmental Engineering, Department of Biology, Faculty of Science and Technology, Universitas Airlangga, Kampus C UNAIR, Jalan Mulyorejo, Surabaya 60115, Indonesia
6 Research Group of Sustainable Environmental Systems and Infrastructure (SUSTAIN), Faculty of Science and Technology, Universitas Airlangga, Kampus C UNAIR, Jalan Mulyorejo, Surabaya 60115, Indonesia
7 Department of Water Management, Faculty of Civil Engineering and Geosciences, Delft University of Technology, Stevinweg 1, 2628 Delft, The Netherlands
* Correspondence: fauzul.imron@fst.unair.ac.id or m.f.imron@tudelft.nl

Abstract

Surfactant adsorption on reservoir rock is a major limitation in chemical enhanced oil recovery (EOR) because it reduces effective surfactant concentration and increases chemical loss. In this study, a sodium lignosulfonate (SLS)-silica nanoparticle (SNP) system was investigated on Buff Berea Sandstone (BBS) at different temperature mitigations to evaluate its potential for adsorption. Residual surfactant concentration was determined by UV-Vis spectrophotometry at 208 nm, yielding excellent linearity R^2 = 0.9948. Adsorption equilibrium was analyzed using Langmuir and the Freundlich isotherm models, while kinetics were evaluated using pseudo-first-order (PFO) and pseudo-second-order (PSO) models. At 30 °C, adsorption was best described by the Langmuir model (R^2 = 0.9619, *SSE* = 2.09, whereas at 60 °C, the Freundlich model gave the best fit (R^2 = 0.8220, *SSE* = 0.36). The optimum SNP concentration increased from 1000 to 1500 mg/L at 30 °C to 2000–2500 mg/L at 60 °C, likely due to elevated temperature, which enhanced molecular mobility and interfacial heterogeneity, thereby requiring more SNPs to cover or shield active adsorption sites on BBS. Kinetic results consistently favored the PSO model. These findings show that SNPs effectively reduce SLS adsorption and modify the adsorption behavior in a temperature-dependent manner, providing useful insight for the design of more efficient chemical-enhanced oil recovery formulations.

Keywords: adsorption kinetics; enhanced oil recovery; resource optimization; silica nanoparticles; sodium lignosulfonate; temperature

Academic Editors: Juan García Rodríguez and Vassilis J. Inglezakis

Received: 10 April 2026
Revised: 25 April 2026
Accepted: 6 May 2026
Published: 7 May 2026

1. Introduction

Surfactant flooding is one of the most established chemical enhanced oil recovery (EOR) methods because it improves oil displacement by reducing interfacial tension (IFT) and facilitating emulsion formation. Despite these advantages, its field-scale application remains limited by substantial surfactant loss due to adsorption onto reservoir rock surfaces, particularly in sandstone systems such as Berea sandstone [1–4]. This adsorption reduces the effective surfactant concentration available for oil mobilization, increases chemical consumption, and ultimately lowers the process's economic feasibility [1,5]. The problem becomes more severe under reservoir conditions characterized by high salinity, elevated temperature, and significant clay content, where electrostatic attraction, hydrophobic interaction, and surface heterogeneity collectively promote stronger surfactant retention on the rock surface [2,6,7].

In recent years, silica nanoparticles (SiO_2) have emerged as promising additives for improving surfactant-based EOR formulations [8,9]. Their attractiveness stems from several practical advantages, including natural abundance, relatively low production costs, environmental compatibility, and nanoscale dimensions that enable transport through porous media with a lower risk of severe pore blockage [10–12]. More importantly, silica nanoparticles exhibit tunable surface chemistry, allowing their interfacial behavior and dispersion stability to be adjusted through surface modification processes such as silanization [10,13–15]. These features make silica nanoparticles particularly attractive for integration into surfactant systems designed for harsh reservoir environments.

The beneficial role of silica nanoparticles in EOR is widely associated with their ability to enhance the stability of foams and emulsions. When adsorbed at the oil-water interface, SiO_2 particles can form a denser, more mechanically resistant interfacial film, thereby reducing interfacial free energy and suppressing coalescence [16–21]. Likewise, control over the density of surface silanol groups has been reported to promote the formation of stable oil-in-water emulsions, thereby improving microscopic sweep efficiency in sandstone reservoirs [11,22–26]. These interfacial effects are particularly relevant under thermally and chemically challenging conditions, where conventional surfactant systems often suffer from rapid destabilization [18,27,28].

Beyond interfacial stabilization, silica nanoparticles have also shown strong potential to suppress surfactant adsorption onto mineral surfaces [29,30]. This improvement is generally attributed to competitive adsorption, steric hindrance, and nanoparticle accumulation along pore walls, all of which reduce direct contact between surfactant molecules and the rock surface [10,27,29]. In addition, silica nanoparticles may alter reservoir wettability from oil-wet to water-wet conditions via the disjoining pressure mechanism, thereby facilitating oil detachment and improving displacement efficiency [22,31–33]. Although these mechanisms have been increasingly reported, the existing literature remains focused primarily on general nanoparticle-assisted surfactant systems.

Previous studies have applied silica nanoparticles to various surfactant-based EOR systems, including surfactant–polymer formulations, anionic surfactants, foam/emulsion systems, and natural/nonionic surfactants [10,27,29,34]. These studies generally demonstrated that silica nanoparticles can reduce surfactant adsorption, improve interfacial stability, alter wettability, and enhance oil recovery. These investigations also primarily focused on conventional synthetic surfactants such as alkylbenzene sulfonates and methyl ester sulfonates [27,29,34]. In these systems, the adsorption-reduction mechanisms, such as competitive adsorption, steric hindrance, and wettability alteration, are relatively well established. However, the behavior of bio-based surfactants, particularly sodium lignosulfonate (SLS), in nanoparticle-assisted systems remains insufficiently explored. This is a critical gap because SLS possesses a more complex and heterogeneous molecular structure, which can

lead to different adsorption characteristics compared to synthetic surfactants. Furthermore, although temperature strongly influences surfactant–rock interactions, nanoparticle stability, and adsorption thermodynamics, systematic investigations of temperature-dependent adsorption behavior in SLS–nanoparticle systems remain lacking. Most existing studies report adsorption performance at a single temperature, thereby limiting the understanding of how adsorption mechanisms evolve under realistic reservoir conditions.

Therefore, this study aims to investigate the adsorption behavior of an SLS–SiO_2 nanoparticle system on Buff Berea Sandstone (BBS) across different temperature conditions. Specifically, BBS was selected as the representative sandstone medium because it is widely used as a reference porous material in EOR-related laboratory studies, has relatively homogeneous petrophysical properties, and provides a higher-permeability sandstone system suitable for evaluating surfactant adsorption and nanoparticle-assisted adsorption mitigation [35,36]. The novelty of this work lies in the use of a low-cost, renewable surfactant (SLS) in combination with silica nanoparticles, the systematic evaluation of temperature-dependent adsorption mechanisms, and the integration of isotherm and kinetic modeling to elucidate changes in adsorption behavior. The findings provide new insights into the design of environmentally sustainable and temperature-resilient surfactant formulations for chemical EOR applications. From a practical perspective, the adsorption-mitigation data obtained in this study can serve as preliminary formulation-screening information for designing SLS–SNP chemical slugs with reduced surfactant loss [1,5,10,30], which can be further validated through core-flooding experiments and reservoir-condition testing prior to field-scale implementation.

2. Materials and Methods

2.1. Materials

Commercial sodium lignosulfonate (SLS) (Domsjö Fabriker AB, Domsjö, Sweden) was used as the surfactant, with a purity of >93%. Silica nanoparticles (SNPs), namely Silica Fumed HDK (Wacker) (Hubei Huifu Nanomaterial, Yichang, China), were used as adsorption-mitigating additives. The SNPs had an average particle size of 20 nm, a BET surface area of 175–225 m^2/g, and a purity of >99.8%. Buff Berea Sandstone (BBS) (ITB, Indonesia) was used as the adsorbent medium to represent sandstone reservoir rock. The BBS was characterized by a permeability of 150–350 mD (KCl) and 400–500 mD (N_2), a porosity of 20–22%, and an unconfined compressive strength (UCS) of 3800–4500 psi. A 3% (*w*/*v*) NaCl solution was used as the solvent for SLS preparation and was prepared from commercial-grade industrial salt. The main laboratory equipment used in this work included volumetric flasks, graduated cylinders, test tubes, volumetric pipettes, dropper pipettes, sample bottles, and centrifuge tubes. Absorbance measurements were performed using a UV–Vis spectrophotometer (Jasco V-730, Tsukuba, Japan). Homogenization of the surfactant–nanoparticle mixtures was carried out using an ultrasonic processor (PZ-LI series, Henan Chuanghe Laboratory Equipment, Zhengzhou, China), while phase separation after adsorption was performed using a centrifuge (Biobase, BKC-TH18, Jinan, China). SNP concentrations in the range of 500–2500 mg/L were selected to determine the saturation point and evaluate the effectiveness of nanoparticle addition in covering active adsorption sites on the rock surface under different temperature conditions. Concentrations of NaCl are reported in % (*w*/*v*), while SLS and SNP concentrations are expressed in mg/L.

2.2. Preparation of SLS Calibration Standards

SLS calibration solutions were prepared at concentrations of 0, 2500, 5000, 7500, 10,000, and 12,500 mg/L using a 30,000 mg/L NaCl solution prepared from commercial-grade industrial salt as the solvent. The absorbance of each standard solution was mea-

sured at 208 nm using the UV–Vis spectrophotometer. These measurements were used to establish the calibration curve for determining the residual SLS concentration in the adsorption experiments.

2.3. Preparation of SLS–SNP Dispersions and Adsorption Experiments

A 5000 mg/L SLS solution was mixed with SNPs at concentrations of 500, 1000, 1500, 2000, and 2500 mg/L and homogenized using an ultrasonic processor for 15 min to obtain a uniform SLS–SNP dispersion. Subsequently, 1 g of BBS was placed into a test tube, followed by the addition of 10 mL of the prepared SLS–SNP mixture. Adsorption experiments were conducted at 30 and 60 °C with contact times ranging from 0 to 9 h. The two temperature points were selected to provide an initial comparison between near-ambient and moderately elevated thermal conditions. The temperature of 30 °C was used as a baseline condition, while 60 °C was selected to represent an elevated condition relevant to thermally influenced reservoir environments [19,27,28], and to evaluate whether higher temperature could alter the adsorption behavior of the SLS–SNP system. This temperature selection was not intended to represent a complete thermal optimization study, but rather to identify the sensitivity of SLS adsorption mitigation by SNPs under two contrasting temperature conditions. After the designated contact time, the suspension was centrifuged at 1000 rpm for 10 min to separate BBS particles and larger suspended solids from the liquid phase. The collected supernatant was then analyzed by UV–Vis spectrophotometry at 208 nm to determine the apparent residual SLS concentration. It should be noted that this centrifugation condition was not intended to completely sediment primary 20 nm SNPs; therefore, possible residual nanoparticle-related scattering or baseline contributions were considered methodological limitations of the present study. The equilibrium adsorption capacity (q_e) was calculated using Equation (1).

$$q_e = (C_0 - C_e)\frac{V}{m} \quad (1)$$

where C_0 and C_e are the initial and the equilibrium concentration of SLS (mg/L), respectively. V is the volume of the SLS–SNP solution (L), and m is the mass of BBS (g) [2].

2.4. Adsorption Isotherm Modeling

Adsorption isotherms were used to evaluate the equilibrium behavior of the SLS–SNP system on BBS. In general, adsorption isotherms describe the relationship between the amount of adsorbate retained on the adsorbent surface and the residual concentration of adsorbate remaining in solution at constant temperature [37]. In this study, the experimental data were interpreted using the Langmuir and the Freundlich isotherm models. The Langmuir isotherm assumes monolayer adsorption on a homogeneous surface with a finite number of energetically equivalent active sites, with no interaction between adsorbed molecules. The nonlinear Langmuir equation is given in Equation (2).

$$q_e = \frac{q_{max} K_L C_e}{1 + K_L C_e} \quad (2)$$

where q_e is the equilibrium adsorption capacity (mg/g), q_{max} is the maximum adsorption capacity (mg/g), C_e is the equilibrium adsorbate concentration (mg/L), and K_L is the Langmuir equilibrium constant (L/mg). For linear analysis, the Langmuir equation may be expressed by plotting $\frac{1}{q_e}$ versus $\frac{1}{C_e}$, which yields a straight line with a slope of $\frac{1}{q_{max} K_L}$

and an intercept of $\frac{1}{q_{max}}$ [38]. The Freundlich isotherm describes non-ideal, reversible, and multilayer adsorption on heterogeneous surfaces. The model is expressed in Equation (3).

$$q_e = bC_e{}^{1/n} \tag{3}$$

where b is the Freundlich constant associated with adsorption capacity and $1/n$ is the heterogeneity factor related to adsorption intensity. The linearized form of the Freundlich model is given in Equation (4).

$$logq_e = logb + \frac{1}{n}logC_e \tag{4}$$

A value of $1/n$ within the range of 0.1–0.5 generally indicates favorable adsorption, whereas a value greater than 0.5 suggests less favorable adsorption behavior. The adequacy of the isotherm models was evaluated using the coefficient of determination (R^2) and the sum of squared errors (SSE) [37].

2.5. Adsorption Kinetic Modeling

Adsorption kinetics were analyzed to provide insight into the adsorption mechanism and the rate-controlling step of SLS–SNP uptake on BBS. In this study, the kinetic behavior was interpreted using the pseudo-first-order (PFO) and pseudo-second-order (PSO) models [2,39–42].

The PFO model assumes that the adsorption rate is proportional to the number of unoccupied adsorption sites and is commonly used to describe physical adsorption processes at the solid–liquid interface [43]. The rate expression is given in Equation (5).

$$\frac{dq_t}{dt} = k_1(q_e - q_t) \tag{5}$$

where q_t is the adsorption capacity at time t (mg/g), q_e is the equilibrium adsorption capacity (mg/g), and k_1 is the pseudo-first-order rate constant (1/h). Lagergren originally introduced the PFO model to describe the adsorption of aqueous solutions onto solid surfaces [44–48].

The PSO model is widely applied to liquid–solid adsorption systems and assumes that the adsorption rate is proportional to the square of the number of unoccupied sites. The differential form of the model is shown in Equation (6).

$$\frac{dq_t}{dt} = k_2(q_e - q_t)^2 \tag{6}$$

where k_2 is the pseudo-second-order rate constant (g/mg·h). For the linearized PSO model, plotting $\frac{t}{q_t}$ against t yields a straight line with a slope of $\frac{1}{q_e}$, from which q_e and k_2 can be obtained. The initial adsorption rate, h, at t = 0 was calculated using Equation (7) [2].

$$h = k_2q_e{}^2 \tag{7}$$

2.6. Error Analysis and Model Evaluation

The agreement between the experimental data and the fitted isotherm and kinetic models was evaluated using the coefficient of determination (R^2), chi-square (χ^2), and the sum of squared errors (SSE). These parameters were used to assess the goodness of fit and the distribution of prediction errors. The corresponding equations are presented in Equations (8)–(10).

$$R^2 = 1 - \frac{\sum_{i=1}^{N}\left(q_{e,\,exp} - q_{e,pred}\right)^2}{\sum_{i=1}^{N}\left(q_{e,\,exp} - \overline{q_{e,exp}}\right)^2} \tag{8}$$

$$\chi^2 = \sum_{i=1}^{N} \left[\frac{\left(q_{e,\,exp} - q_{e,pred}\right)^2}{q_{e,\,exp}} \right] \quad (9)$$

$$SSE = \sum_{i=1}^{N} \left(q_{e,\,exp} - q_{e,pred}\right)^2 \quad (10)$$

In addition to R^2, χ^2, and SSE, the reduced chi-square (χ^2_{red}) and root mean square error (RMSE) were also used to further evaluate the goodness of fit of the isotherm models. The reduced chi-square was calculated by normalizing χ^2 to the degree of freedom, as shown in Equation (11), while RMSE was calculated using Equation (12). These additional error functions are useful because R^2 alone may not fully represent the distribution of residual errors in nonlinear adsorption modeling [49–51].

$$\chi^2_{red} = \frac{\chi^2}{N - p} \quad (11)$$

$$RMSE = \sqrt{\frac{\sum_{i=1}^{N} (q_{e,exp} - q_{e,pred})^2}{N - p}} \quad (12)$$

where $q_{e,exp}$ and $q_{e,pred}$ are the experimental and model-predicted adsorption capacities, respectively, $\bar{q}_{e,exp}$ is the mean experimental adsorption capacity, and N is the number of experimental data points, and p is the number of fitted model parameters. For both the Langmuir and the Freundlich models used in this study, $p = 2$. The uncertainty of q_e was expressed as the standard deviation of repeated measurements and presented as error bars in the isotherm plots.

3. Results and Discussion

3.1. Standard Curve

The standard curve was obtained by analyzing SLS standard solutions using UV–Vis spectrophotometry at the maximum wavelength (λ_{max}) of 208 nm (Figure 1).

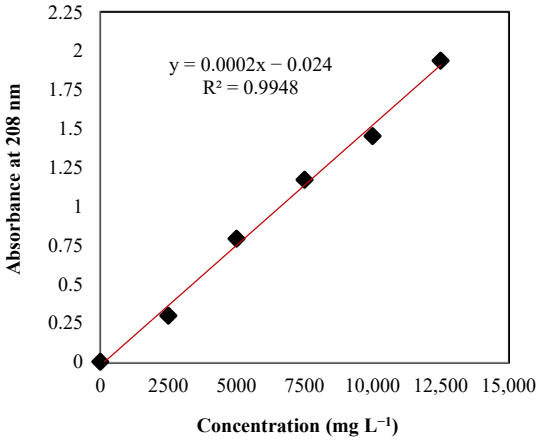

Figure 1. Standard calibration curve for SLS–SNP adsorption analysis on BBS.

Based on Figure 1, a linear regression equation of y = 0.0002x − 0.024 was obtained, with a coefficient of determination (R^2) of 0.9948. This result indicates a strong linear relationship between concentration and absorbance within the studied range. The regression equation was subsequently used to determine the residual SLS–SNP concentration during the adsorption experiments. Because residual nanoscale silica particles may remain in the supernatant after low-speed centrifugation, possible light scattering or baseline contribution during UV–Vis measurement cannot be fully excluded. Therefore, the

residual SLS concentration obtained in this study should be interpreted as an apparent UV–Vis-based concentration after BBS separation. Nevertheless, all treatment samples were processed under the same separation and measurement conditions; therefore, the comparative adsorption trends among SNP concentrations remain useful for evaluating the adsorption-mitigation effect of SNPs. Future studies should include high-speed centrifugation, ultrafiltration, or SNP-containing blank correction to minimize nanoparticle-related optical interference further.

3.2. Langmuir and Freundlich Adsorption Isotherm Modeling

The adsorption isotherm behavior of the SLS–SNP system on BBS was evaluated using the Langmuir and the Freundlich models. For improved comparison, the nonlinear fitting curves at 30 and 60 °C are presented together in Figure 2. At 30 °C, the Langmuir model provided a slightly better fit than the Freundlich model, as indicated by a higher R^2 and a lower *SSE*. In contrast, at 60 °C, the Freundlich model showed better agreement with the experimental data than the Langmuir model. This comparison indicates that the adsorption behavior shifted from predominantly Langmuir-type adsorption at 30 °C to more heterogeneous Freundlich-type adsorption at 60 °C.

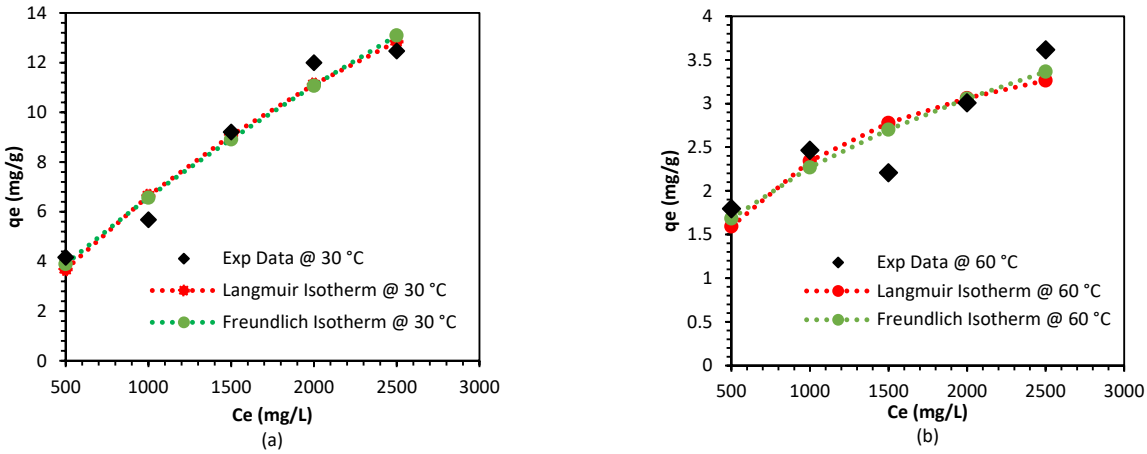

Figure 2. Nonlinear Langmuir and Freundlich isotherm fitting for the adsorption of the SLS–SNP system on BBS at different temperatures: (**a**) 30 °C and (**b**) 60 °C.

As shown in Table 1, in the Langmuir model, a higher K_L value indicates a stronger interaction between the adsorbate and the adsorbent. In the Freundlich model, adsorption is considered favorable when the value of $1/n$ is within the range of 0.1–0.5, whereas a value greater than 0.5 suggests less favorable adsorption behavior [2,38]. The suitability of each isotherm model was evaluated based on the highest R^2 value and the lowest *SSE* value, which indicate better agreement between the model and the experimental data [2].

Table 1. Isotherm parameters for the adsorption of the SLS–SNP system on BBS at different temperatures.

Temperature (°C)	Model	Isotherm Parameters		Fitting Indicators			
				R^2	*SSE*	χ^2_{red}	RMSE
30	Langmuir	K_L = 0.000242 L/mg	q_{max} = 34.0632 mg/g	0.9619	2.09	0.0991	0.3736
30	Freundlich	K_F = 0.0361	n = 1.3276	0.9600	0.51	0.0894	0.3829
60	Langmuir	K_L = 0.001126 L/mg	q_{max} = 4.4220 mg/g	0.7483	2.19	0.0703	0.1838
60	Freundlich	K_F = 0.1161	n = 2.3246	0.8220	0.36	0.0502	0.1546

Based on these criteria, the Langmuir isotherm best describes the adsorption of the SLS–SNP system on the BBS surface at 30 °C, with an R^2 value of 0.9619 and an SSE value of 2.09. In contrast, at 60 °C, the Freundlich isotherm provides a better representation of the adsorption process, with an R^2 value of 0.8220 and an SSE value of 0.36.

The fitting quality of the isotherm models was further evaluated using additional error indicators, including reduced chi-square (χ^2_{red}) and RMSE, as summarized in Table 1. These parameters were included because the coefficient of determination alone may be insufficient to assess nonlinear adsorption models, particularly when residual errors are not uniformly distributed. At 30 °C, the Langmuir model showed the best agreement with the experimental data, as indicated by the highest R^2 value and the lowest error indicators. In contrast, at 60 °C, the Freundlich model provided a better fit, confirming that elevated temperature promoted a more heterogeneous adsorption behavior of the SLS–SNP system on BBS.

A slight deviation of one experimental point from the general isotherm trend was observed in the fitted curve. Because no data point was removed during nonlinear fitting, this deviation was retained and discussed as part of the actual adsorption response of the SLS–SNP–BBS system. The deviation may be attributed to the complex interfacial behavior of the nanoparticle-assisted surfactant system, including competitive adsorption between SLS and SNPs, partial blocking of surface sites by nanoparticles, possible nanoparticle–surfactant association, and the heterogeneous mineral surface of BBS. Therefore, the deviation was interpreted as system-specific adsorption behavior rather than being arbitrarily treated as an outlier.

The transition from Langmuir-dominated behavior at 30 °C to Freundlich-dominated behavior at 60 °C indicates that increasing temperature altered the adsorption environment of the SLS–SNP system on BBS. At 30 °C, the adsorption process was more consistent with a finite-site mechanism, in which SLS retention occurred mainly on relatively uniform active sites, and SNPs could effectively shield or block direct SLS–rock interactions. At 60 °C, increased thermal motion may enhance the mobility of SLS molecules and SNPs, promote repeated adsorption–desorption events, and modify SLS–SNP association near the sandstone surface. These processes can broaden the distribution of adsorption energies and increase interfacial heterogeneity, making the Freundlich model more suitable. Thus, the Freundlich behavior at elevated temperature should be viewed primarily as an indication of non-ideal adsorption on heterogeneous sites, rather than definitive proof of a well-ordered multilayer adsorption structure [10,27,29,48].

In addition to model suitability, the adsorption capacity values provide important information on the extent of SLS retention on the BBS surface. As shown in Table 1, the Langmuir maximum adsorption capacity (q_{max}) of the SLS–SNP system was 34.0632 mg/g at 30 °C and decreased to 4.4220 mg/g at 60 °C. In chemical EOR, lower surfactant adsorption is desirable because it indicates lower surfactant loss to the rock surface and a higher fraction of surfactant remaining available in the injected fluid. Therefore, the reduced adsorption capacity under SNP-assisted conditions supports the role of silica nanoparticles as adsorption-mitigation additives rather than as conventional adsorbents for surfactant removal.

Compared with previous lignosulfonate adsorption studies, the obtained q_{max} values are within the reported range for mineral- and waste-derived adsorbents. Zulfikar et al. reported lignosulfonate adsorption capacities of 93.46 mg/g for powdered eggshell, 6.08 mg/g for Berea sandstone, 1.646 mg/g for limestone, 0.534 mg/g for dolomite, 0.42 mg/g for activated charcoal, 0.177 mg/g for wood ash, and 233.1 mg/g for sepiolite [52]. This wide variation confirms that lignosulfonate adsorption is strongly affected by adsorbent mineralogy, surface area, surface charge, and solution chemistry. However,

unlike wastewater treatment applications, where high adsorption capacity is targeted for pollutant removal, the objective in surfactant-based EOR is to minimize surfactant retention. Thus, the lower adsorption capacity observed under optimized SNP addition indicates that SNPs contributed to suppressing direct SLS adsorption onto BBS. This interpretation is consistent with previous nanoparticle-assisted EOR studies showing that silica nanoparticles can reduce surfactant adsorption through competitive adsorption, surface-site blocking, and modification of surfactant–rock interactions [10,27,29,53].

3.3. Determination of the Optimum SNP Concentration in the Adsorption Process

Recent studies have shown that adding silica nanoparticles can reduce surfactant adsorption on rock surfaces, thereby improving oil recovery efficiency. In addition, SNPs may modify interfacial tension, increase solution viscosity, and enhance the thermal stability of surfactants during the EOR process [54]. In the present study, the optimal SNP concentration in the SLS solution was determined by analyzing the adsorption capacity of the SLS–SNP system at 30 and 60 °C over specific contact times.

Based on Figure 3a, the SNP concentration range of 1000–1500 mg/L can be considered optimal for the adsorption process at 30 °C. This is indicated by the lower adsorption capacity (q_e) values within this concentration range compared with those of the SLS solution without SNP addition. These results demonstrate that the addition of SNPs at 1000–1500 mg/L effectively reduces surfactant adsorption on the rock surface under these temperature conditions. Based on Figure 3b, the optimum SNP concentration range at 60 °C was identified as 2000–2500 mg/L. The higher optimum SNP concentration at 60 °C may be attributed to increased molecular mobility and greater interfacial heterogeneity at elevated temperature. Under this condition, the interactions among SLS molecules, SNPs, and the BBS surface become more dynamic, so a higher SNP dosage is required to effectively cover or shield active adsorption sites and suppress direct SLS adsorption onto the sandstone surface [27,29].

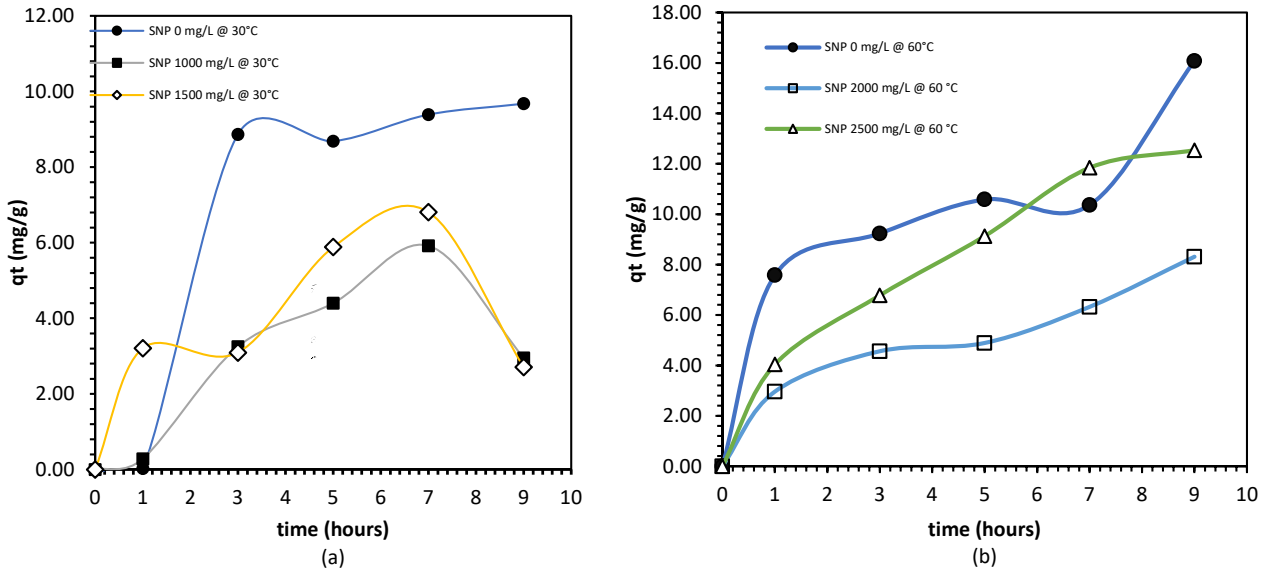

Figure 3. Adsorption capacity profiles of the SLS–SNP system on BBS at different temperatures: (**a**) 30 °C with SNP concentrations of 0, 1000, and 1500 mg/L; and (**b**) 60 °C with SNP concentrations of 0, 2000, and 2500 mg/L.

This conclusion is based on the lower q_e values observed at these concentrations relative to the adsorption capacity of the SLS solution without SNP addition. Therefore, the addition of SNPs within this range was effective in suppressing surfactant adsorption on

the rock surface at elevated temperature. The difference in optimum SNP concentration between 30 and 60 °C suggests that temperature significantly affects the interaction between the nanoparticle-assisted surfactant system and the BBS surface.

The increase in optimum SNP concentration at 60 °C may also be associated with changes in SNP dispersion stability under elevated-temperature saline conditions. At higher temperatures, increased Brownian motion and reduced solution viscosity can increase the collision frequency of nanoparticles, which may promote partial aggregation or reduce the effective number of well-dispersed SNPs available to interact with the sandstone surface. In surfactant–nanoparticle systems, dispersion stability is strongly influenced by the adsorption of surfactant molecules on the silica surface, electrostatic or steric repulsion among particles, salinity, temperature, and particle concentration [18,19]. Therefore, a higher SNP dosage at 60 °C may be required to maintain sufficient dispersed nanoparticles that can shield active adsorption sites and reduce direct SLS adsorption on BBS. This interpretation is consistent with previous studies showing that surfactant-assisted silica nanofluids can maintain better dispersion stability and EOR performance under high-temperature and high-salinity conditions when the nanoparticle–surfactant ratio is properly optimized [27–29].

The transition from Langmuir-type behavior at 30 °C to Freundlich-type behavior at 60 °C further supports the view that higher temperature alters the adsorption environment, leading to more heterogeneous surface interactions and a more complex adsorption mechanism. The comparison with the SLS-only control confirms the adsorption-mitigation effect of SNPs, as the optimized SLS–SNP systems exhibited lower adsorption capacities than the system without SNP addition at both 30 and 60 °C.

The selection of 30 and 60 °C was intended as an initial temperature-screening approach to compare near-ambient and moderately elevated thermal conditions. The clear difference in the optimum SNP concentration between the two temperatures indicates that SNP-mediated adsorption is temperature-dependent. At 30 °C, 1000–1500 mg/L SNP was sufficient to reduce SLS adsorption, whereas at 60 °C, a higher SNP dosage of 2000–2500 mg/L was required. This behavior suggests that elevated temperature may modify surfactant–nanoparticle association, enhance molecular mobility, and increase the heterogeneity of SLS–BBS interactions [27–29]. From an energy and economic perspective, the 60 °C condition should be considered as a simulation of reservoir thermal conditions rather than an additional heating requirement for field application. The main economic relevance of SNP addition is its potential to reduce surfactant retention, maintain effective surfactant concentration, and reduce chemical loss during chemical flooding [1,5,10]. Nevertheless, the higher SNP dosage required at 60 °C indicates a trade-off between nanoparticle addition and surfactant-saving benefits. Therefore, future work should include a broader temperature range, core-flooding validation, and techno-economic analysis to optimize the SLS–SNP formulation for specific reservoir conditions.

3.4. Adsorption Kinetic Models

Adsorption kinetics were analyzed to evaluate the adsorption rate and to provide insight into the rate-controlling mechanism of the process. In this study, non-linear kinetic models were used to analyze the adsorption behavior of the SLS–SNP system on BBS. The adsorption data were first fitted using the pseudo-first-order (PFO) model. Model suitability was evaluated by comparing the experimental and calculated adsorption capacities and by examining the chi-square (χ^2) and coefficient of determination (R^2) values, where lower (χ^2) and higher (R^2) values indicate better model performance [55].

Figure 4 shows the PFO kinetic fitting for the adsorption of the SLS–SNP system on BBS at 30 and 60 °C, respectively. At 30 °C, the system containing 1000 mg/L SNP followed

the PFO model only during the initial contact period of 0–3 h, while the 1500 mg/L system showed agreement with the PFO model only during the first 2 h. In contrast, at 60 °C, the systems containing 2000 and 2500 mg/L SNP exhibited closer agreement with the PFO model over a broader contact-time range.

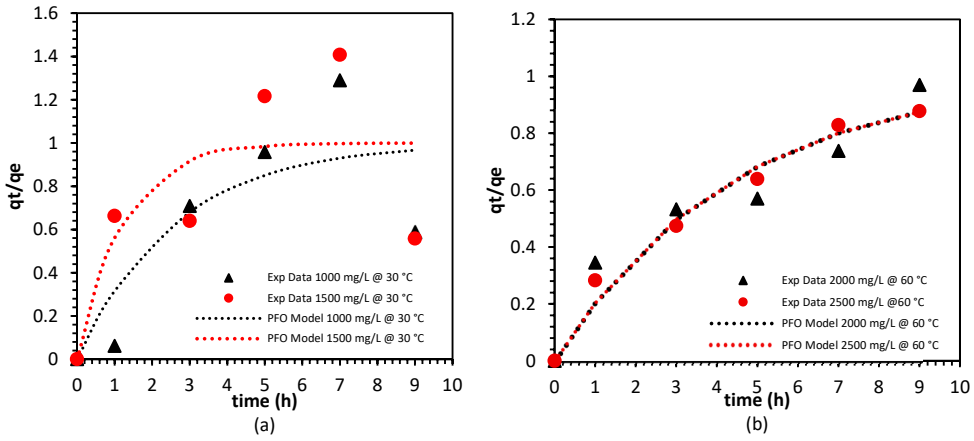

Figure 4. Pseudo-first-order kinetic fitting for the adsorption of the SLS–SNP system on BBS at different temperatures: (**a**) 30 °C and (**b**) 60 °C.

Figure 5 presents the pseudo-second-order (PSO) kinetic fitting for the adsorption process at 30 and 60 °C, respectively. Overall, the adsorption kinetic data were better described by the PSO model than by the PFO model, regardless of adsorption temperature or SNP concentration.

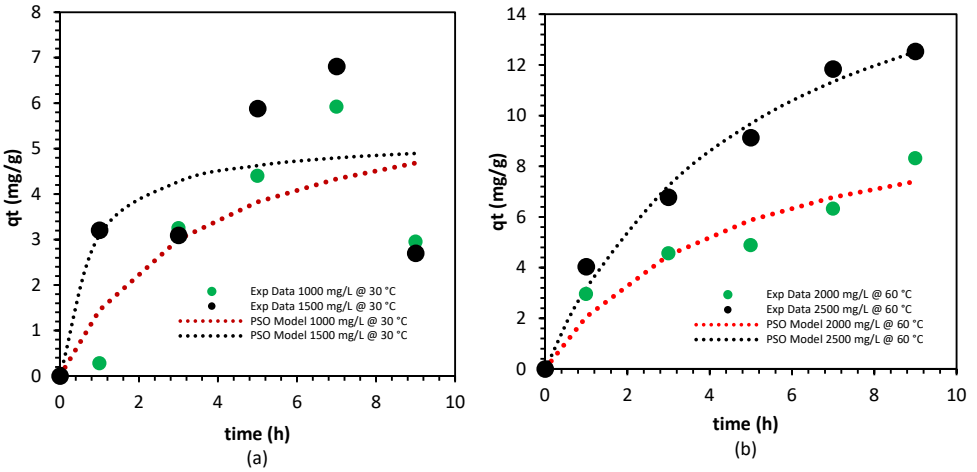

Figure 5. Pseudo-second-order kinetic fitting for the adsorption of the SLS–SNP system on BBS at different temperatures: (**a**) 30 °C and (**b**) 60 °C.

Based on the kinetic parameters summarized in Table 2, the PSO model provided a better overall fit to the experimental adsorption data, as indicated by the lower χ^2 values and generally higher R^2 values at both 30 and 60 °C. In addition, the PSO model showed a stronger correspondence between experimental and predicted adsorption behavior than the PFO model did. Although some deviation between experimental and modeled q_e values remained, the goodness-of-fit parameters consistently favored the PSO model. The kinetic parameters obtained from the PFO and PSO models are summarized in Table 2. For clearer comparison, the parameters were reorganized according to temperature, SNP concentration, and kinetic model.

Table 2. Kinetic parameters for the adsorption of the SLS–SNP system on BBS at different temperatures.

Model	Temperature (°C)	SNP Concentration (mg/L)	q_e (Exp) (mg/g)/q_e (Model) (mg/g)	Rate Constant	Fitting Indicator
PFO	30	1000	5.9185/4.5891	k_1 = 0.3792 h^{-1}	R^2 = 0.6128; SSE = 7.38; χ^2 = 6.50
PFO	30	1500	6.8079/4.3891	k_1 = 0.8231 h^{-1}	R^2 = 0.2906; SSE = 11.78; χ^2 = 3.13
PFO	60	2000	8.3121/8.5730	k_1 = 0.2303 h^{-1}	R^2 = 0.8317; SSE = 3.41; χ^2 = 0.82
PFO	60	2500	12.5369/14.2934	k_1 = 0.2296 h^{-1}	R^2 = 0.9687; SSE = 1.91; χ^2 = 0.30
PSO	30	1000	5.9185/6.4934	k_2 = 0.0442 g/mg·h	R^2 = 0.7288; SSE = 7.24; χ^2 = 6.30
PSO	30	1500	6.8079/10.4301	k_2 = 0.0228 g/mg·h	R^2 = 0.8906; SSE = 3.13; χ^2 = 0.97
PSO	60	2000	8.3121/10.9584	k_2 = 0.0211 g/mg·h	R^2 = 0.8610; SSE = 2.82; χ^2 = 0.60
PSO	60	2500	12.5369/19.7948	k_2 = 0.0097 g/mg·h	R^2 = 0.9702; SSE = 1.49; χ^2 = 0.26

As shown in Table 2, the PSO model provided a better overall fit than the PFO model under all investigated conditions. This is indicated by the generally higher R^2 values and lower SSE and χ^2 values obtained from the PSO model. Therefore, the adsorption kinetics of the SLS–SNP system on BBS were more appropriately described by the PSO model at both 30 and 60 °C. These results suggest that the adsorption of the SLS–SNP system on BBS is governed predominantly by PSO-type kinetic behavior. Mechanistically, the better agreement of the PSO model indicates that the adsorption rate was not controlled solely by simple diffusion or physical occupation of vacant sites, but by interaction-dependent surface processes involving SLS molecules, SNPs, and the BBS surface [48]. SLS may interact with sandstone through electrostatic attraction, hydrophobic association, and mineral surface interactions, while SNPs can compete for active adsorption sites, shield the rock surface, and reduce direct SLS–rock contact. In addition, the silanol-rich surface of SiO_2 may facilitate SLS–SNP association through hydrogen bonding, electrostatic interaction, and steric stabilization [10,27,29]. Therefore, the PSO fit supports the interpretation that adsorption mitigation in this system arises from coupled SLS–SNP–rock interactions rather than a single-step physical adsorption process. Nevertheless, the PSO model should not be interpreted as definitive proof of purely chemical adsorption; rather, it indicates that the overall adsorption rate is better described by an interaction-controlled kinetic process.

3.5. Limitations of This Study and Future Research Perspective

The present study provides an initial adsorption-screening assessment of the SLS SNP system on BBS by evaluating the effects of SNP concentration and temperature on surfactant adsorption mitigation. These findings support the role of SNPs as adsorption-mitigation additives for SLS-based chemical EOR systems [10,27,29]. Nevertheless, the scope of this study remains limited to static adsorption experiments conducted at two temperatures. Further investigation is required to improve the reliability and field relevance

of the SLS–SNP formulation. Future studies should evaluate a broader range of reservoir-related parameters, including salinity, pH, divalent ion concentration, nanoparticle size, SNP surface charge, and surfactant concentration. In addition, interfacial tension, contact angle, zeta potential, dispersion stability, and core-flooding tests should be conducted to directly link adsorption mitigation with wettability alteration, displacement efficiency, and oil recovery performance [22,27,31]. These additional experiments would provide a more comprehensive understanding of the SLS–SNP–rock interaction and support the development of more robust and economically viable chemical EOR formulations. In addition, further methodological refinement, such as high-speed centrifugation, ultrafiltration, or SNP-containing blank correction, is recommended to minimize potential nanoparticle-related optical interference during UV–Vis quantification.

4. Conclusions

This study demonstrated that silica nanoparticles can effectively reduce the adsorption of sodium lignosulfonate (SLS) onto Buff Berea Sandstone (BBS), thereby supporting the development of more efficient surfactant-based chemical EOR formulations. The UV–Vis calibration curve at 208 nm showed strong linearity, confirming the suitability of the analytical method for determining the residual SLS concentration under the experimental conditions used. Adsorption isotherm analysis revealed that the adsorption process at 30 °C was better described by the Langmuir model, indicating adsorption on relatively homogeneous finite sites, whereas at 60 °C the Freundlich model provided a better fit, suggesting a shift toward more heterogeneous adsorption behavior. The optimum SNP concentration for suppressing SLS adsorption increased from 1000 to 1500 mg/L at 30 °C to 2000–2500 mg/L at 60 °C, indicating that elevated temperature requires a higher nanoparticle dosage to maintain effective adsorption mitigation. Kinetic modeling further showed that the pseudo-second-order model consistently provided a better fit than the pseudo-first-order model, suggesting that adsorption mitigation was governed by interaction-dependent processes involving SLS molecules, SNPs, and the BBS surface.

From a practical perspective, the results indicate that SNPs can be used as adsorption-control additives in SLS-based chemical EOR systems to reduce surfactant loss and maintain a higher effective surfactant concentration in the injected fluid. This finding is particularly relevant to the design of surfactant–nanoparticle chemical slugs under reservoir conditions, where temperature affects surfactant retention and nanoparticle performance. However, the present study should be considered an initial batch adsorption-screening assessment rather than a complete field-scale validation. Future research should investigate broader reservoir-related parameters, including wider temperature ranges, salinity, pH, divalent ions, surfactant concentration, nanoparticle size, and SNP dispersion stability. In addition, interfacial tension, contact angle, zeta potential, and long-term nanofluid stability measurements should be conducted to directly link the mitigation of adsorption to wettability alteration, interfacial behavior, and formulation stability. Core-flooding experiments and techno-economic analysis are also recommended to assess whether the reduced SLS adsorption observed in batch systems translates into improved oil displacement efficiency and economically viable field-scale chemical EOR performance. However, this study was limited to static adsorption experiments at two temperature conditions. Future work should include broader reservoir-condition parameters, interfacial property measurements, and core-flooding validation to directly correlate adsorption mitigation with oil recovery performance and economic feasibility.

Author Contributions: S.D.: Supervision, validation, data curation, writing—original draft; P.M.: Investigation, formal analysis, data curation; S.A.R.: Investigation, formal analysis, writing—original draft; A.H.: writing—original draft; H.A.: writing—original draft; F.C.S.: data curation; S.B.K.:

data curation, visualization, validation, writing—original draft, writing—review and editing; M.F.I.: funding acquisition, writing—review and editing. All authors have read and agreed to the published version of the manuscript.

Funding: The authors gratefully acknowledge the financial support provided by the Institute for Research and Community Service, Universitas Singaperbangsa Karawang (UNSIKA), through its internal competitive research grant scheme. The APC was funded by TU Delft.

Institutional Review Board Statement: Not applicable.

Informed Consent Statement: Not applicable.

Data Availability Statement: The original contributions presented in this study are included in the article. Further inquiries can be directed to the corresponding author.

Acknowledgments: During the preparation of this manuscript/study, the authors used Grammarly 1.156.1.0 and ChatGPT 5.3 for the purposes of language refinement. The authors have reviewed and edited the output and take full responsibility for the content of this publication.

Conflicts of Interest: The authors declare no conflicts of interest.

References

1. Koparal, G.B.; Sharma, H.; Liyanage, P.J.; Panthi, K.K.; Mohanty, K.K. Reducing Surfactant Retention Using Polyacrylate in Berea Sandstone. *J. Pet. Sci. Eng.* **2022**, *208*, 109228. [CrossRef]
2. Yusuff, A.S.; Gbadamosi, A.O.; Bode-Olajide, F.B.; Igbafe, A.I. Adsorption of Methyl Ester Sulfonate Surfactant on Berea Sandstone: Parametric Optimization, Kinetics, Isotherm and Thermodynamics Studies. *Colloids Surf. A Physicochem. Eng. Asp.* **2024**, *686*, 133363. [CrossRef]
3. Al-Wahaibi, Y.; Al-Hashmi, A.A.; Joshi, S.; Mosavat, N.; Rudyk, S.; Al-Khamisi, S.; Al-Kharusi, T.; Al-Sulaimani, H. Mechanistic Study of Surfactant/Polymer Adsorption and Its Effect on Surface Morphology and Wettability. *Soc. Pet. Eng.—SPE Oil Gas India Conf. Exhib.* **2017**, *2017*, 594–609. [CrossRef]
4. Dampang, S.; Azis, M.M.; Yuliansyah, A.T.; Purwono, S. Experimental Investigation of Silica Nanoparticle Assisted Lignosulfonate Surfactant for Chemical Enhanced Oil Recovery (EOR) Flooding. *ASEAN J. Chem. Eng.* **2024**, *24*, 200–209.
5. Liu, Z.; Zhao, G.; Brewer, M.; Lv, Q.; Sudhölter, E.J.R. Comprehensive Review on Surfactant Adsorption on Mineral Surfaces in Chemical Enhanced Oil Recovery. *Adv. Colloid Interface Sci.* **2021**, *294*, 102467. [CrossRef] [PubMed]
6. Panthi, K.; Aitkulov, A.; Mohanty, K.K. Chemical EOR Formulation for a Clay-Rich Sandstone Reservoir with Reduced Surfactant Consumption. *ACS Omega* **2025**, *10*, 1401–1410. [CrossRef]
7. Dampang, S.; Purwanti, E.; Destyorini, F.; Kurniawan, S.B.; Abdullah, S.R.S.; Imron, M.F. Analysis of Optimum Temperature and Calcination Time in the Production of CaO Using Seashells Waste as $CaCO_3$ Source. *J. Ecol. Eng.* **2021**, *22*, 221–228. [CrossRef]
8. Abu Hasan, H.; Muhamad, M.H.; Budi Kurniawan, S.; Buhari, J.; Husain Abuzeyad, O. Managing Bisphenol A Contamination: Advances in Removal Technologies and Future Prospects. *Water* **2023**, *15*, 3573. [CrossRef]
9. Rezvani, H.; Binks, B.P.; Nguyen, D. Surfactant-Nanoparticle Formulations for Enhanced Oil Recovery in Calcite-Rich Rocks. *Langmuir* **2024**, *40*, 24989–25002. [CrossRef]
10. Kesarwani, H.; Sharma, S.; Mandal, A. Application of Novel Colloidal Silica Nanoparticles in the Reduction of Adsorption of Surfactant and Improvement of Oil Recovery Using Surfactant Polymer Flooding. *ACS Omega* **2021**, *6*, 11327–11339. [CrossRef]
11. Tliba, L.; Edokali, M.; Moore, T.; Choudhry, O.; Glover, P.W.J.; Menzel, R.; Hassanpour, A. Spontaneous In-Situ Emulsification and Enhanced Oil Recovery Using Functionalised Silica Nanoparticles: Insights from Spontaneous Imbibition and Micromodel Flooding Tests. *J. Mol. Liq.* **2025**, *424*, 127021. [CrossRef]
12. Kurniawan, S.B.; Purwanti, I.F.; Titah, H.S. The Effect of PH and Aluminium to Bacteria Isolated from Aluminium Recycling Industry. *J. Ecol. Eng.* **2018**, *19*, 154–161. [CrossRef] [PubMed]
13. Barman, J.; Talukdar, P. Using Silica Nanoparticles and Anionic Surfactant in Low-Salinity Water to Enhance Oil Recovery in the Assam Shelf Basin. *J. Pet. Explor. Prod. Technol.* **2025**, *15*, 1190–1208. [CrossRef]
14. Suresh, R.; Kuznetsov, O.; Agrawal, D.; Darugar, Q.; Khabashesku, V. Reduction of Surfactant Adsorption in Porous Media Using Silica Nanoparticles. In Proceedings of the Offshore Technology Conference, Houston, TX, USA, 30 April–3 May 2018; Volume 2, pp. 984–992. [CrossRef]
15. Wibowo, Y.G.; Safitri, H.; Kusumawati; Aini, W.D.; Farantino, R.; Ginting, S.B.; Rinovian, A.; Kurniawan, S.B.; Khairurrijal, K.; Taher, T.; et al. Biochar MMT ZnAl LDH Composite Materials Derived from Solid Waste for Heavy Metal Removal in Artificial Acid Mine Drainage. *Sci. Rep.* **2025**, *15*, 14914. [CrossRef]

16. Jia, H.; Wang, D.; Wang, Q.; Dai, J.; Wang, Q.; Wen, S.; Wang, Z.; Wang, B.; Jiang, X.; Li, X.; et al. The Synthesis of Novel Amphiphilic GOJS-Cn Nanoparticles and Their Further Application in Stabilizing Pickering Emulsion and Enhancing Oil Recovery. *J. Pet. Sci. Eng.* **2022**, *214*, 110537. [CrossRef]
17. Gu, Z.; Lu, T.; Li, Z.; Xu, Z. Experimental Investigation on the SiO2 Nanoparticle Foam System Characteristics and Its Advantages in the Heavy Oil Reservoir Development. *J. Pet. Sci. Eng.* **2022**, *214*, 110438. [CrossRef]
18. Xu, D.; Wen, C.; Wang, L.; Jiang, W.; Kang, W. Mechanisms of SiO_2 Nanoparticles Cooperating with Surfactants to Stabilize Emulsions: Insights from Interfacial Rheological Properties. *J. Mol. Liq.* **2025**, *438*, 128686. [CrossRef]
19. Rezaei, A.; Derikvand, Z.; Parsaei, R.; Imanivarnosfaderani, M. Surfactant-Silica Nanoparticle Stabilized N2-Foam Flooding: A Mechanistic Study on the Effect of Surfactant Type and Temperature. *J. Mol. Liq.* **2021**, *325*, 115091. [CrossRef]
20. Wu, X.; Hou, Z.; Wang, H.; Yang, Y.; Liu, X.; Chen, Z.; Cui, Z. Synergistic Effects between Anionic Surfactant SDS and Hydrophilic Silica Nanoparticles in Improving Foam Performance for Foam Flooding. *J. Mol. Liq.* **2023**, *390*, 123156. [CrossRef]
21. Xinying, W.; Peng, X.; Mingbiao, X.; Lei, P.; Yu, Z. Synergistic Improvement of Foam Stability with SiO2 Nanoparticles (SiO2-NPs) and Different Surfactants. *Arab. J. Chem.* **2023**, *16*, 104394. [CrossRef]
22. Tliba, L.; Edokali, M.; Mehrabi, M.; Glover, P.W.J.; Menzel, R.; Hassanpour, A. Enhancing Oil Recovery with Shape-Modified Silica Nanoparticles: Efficiency in Oil-Wet Sandstone Reservoirs via Imbibition and Micromodel Approaches. *Energy Fuels* **2025**, *39*, 3765–3786. [CrossRef]
23. Tliba, L.; Sagala, F.; Hethnawi, A.; Glover, P.W.J.; Menzel, R.; Hassanpour, A. Surface-Modified Silica Nanoparticles for Enhanced Oil Recovery in Sandstone Cores. *J. Mol. Liq.* **2024**, *413*, 125815. [CrossRef]
24. Khoramian, R.; Ganiyeva, K.; Issakhov, M.; Pourafshary, P.; Aidarova, S.; Sharipova, A. Chemically Surface-Etched Nanoparticles for Tailored Pickering Emulsions in Enhanced Oil Recovery. *J. Mol. Liq.* **2025**, *437*, 128613. [CrossRef]
25. He, M.; Pu, W.; He, Z.; Zheng, L.; Yang, X.; Qian, W. Experimental Study on the Emulsification and Interfacial Properties of Modified Nano-Silica Fluids: Effects of Fatty Acids, Dicarboxylic Acids, Fatty Amines, and Aromatic Acids. *Colloids Surf. A Physicochem. Eng. Asp.* **2026**, *734*, 139428. [CrossRef]
26. Hosny, R.; Zahran, A.; Abotaleb, A.; Ramzi, M.; Mubarak, M.F.; Zayed, M.A.; El Shahawy, A.; Hussein, M.F. Nanotechnology Impact on Chemical-Enhanced Oil Recovery: A Review and Bibliometric Analysis of Recent Developments. *ACS Omega* **2023**, *8*, 46325–46345. [CrossRef] [PubMed]
27. Joshi, D.; Maurya, N.K.; Kumar, N.; Mandal, A. Experimental Investigation of Silica Nanoparticle Assisted Surfactant and Polymer Systems for Enhanced Oil Recovery. *J. Pet. Sci. Eng.* **2022**, *216*, 110791. [CrossRef]
28. Kumar, G.; Mani, E.; Sangwai, J.S. Impact of Surface-Modified Silica Nanoparticle and Surfactant on the Stability and Rheology of Oil-in-Water Pickering and Surfactant-Stabilized Emulsions under High-Pressure and High-Temperature. *J. Mol. Liq.* **2023**, *379*, 121620. [CrossRef]
29. Rahman, A.F.A.; Arsad, A.; Vo, D.V.N.; Bahari, M.B. Nano-Silica to Reduce of Surfactant Adsorption in Oil Recovery: A Review. *Environ. Chem. Lett.* **2025**, *24*, 173–199. [CrossRef]
30. Rahimy, A.; Suramairy, R.; Hasan, D.A.; Khalid, A.W. Nanoparticle-Assisted Surfactant Formulation for High Salinity and Temperature Conditions: Integrated Laboratory Evaluation of Interfacial Properties and Wettability Modification in Carbonates. *Chem. Phys. Impact* **2026**, *12*, 101019. [CrossRef]
31. Seidy-Esfahlan, M. Advancements in Enhanced Oil Recovery with Surface-Modified Silica Nanoparticles: Synthesis, Mechanisms, and Experimental Insights. *J. Mol. Liq.* **2025**, *435*, 128157. [CrossRef]
32. Peng, B.; Gao, H.; Liu, Q.; Yi, P.; Li, Y.; Liu, W.; Xu, Y. On the Role of Disjoining Pressure in Nanofluid-Assisted Enhanced Oil Recovery: A Mini-Review. *RSC Adv.* **2024**, *14*, 23322–23331. [CrossRef] [PubMed]
33. Dampang, S.; Azis, M.M.; Yuliansyah, A.T.; Purwono, S. On the Influence of Silica Nanoparticles for Enhanced Oil Recovery (EOR). In Proceedings of the AIP Conference Proceedings, 2024, Ambon, Indonesia, 9–10 August 2022; Volume 3073.
34. Daghbandan, A.; Shahrabadi, A.; Arabiyoun, M. Adsorption of Glycyrrhiza Glabra Natural Nonionic Surfactant onto the Carbonate Reservoir Rock in the Presence of SiO2 Nanoparticles Surface: Towards Enhanced Oil Recovery. *J. Environ. Chem. Eng.* **2022**, *10*, 107109. [CrossRef]
35. Safari, H.; Balcom, B.J.; Afrough, A. Characterization of Pore and Grain Size Distributions in Porous Geological Samples—An Image Processing Workflow. *Comput. Geosci.* **2021**, *156*, 104895. [CrossRef]
36. Abe, K.; Seddiqi, K.N.; Hou, J.; Fujii, H. Experimental Performance Evaluation and Optimization of a Weak Gel Deep-Profile Control System for Sandstone Reservoirs. *ACS Omega* **2024**, *9*, 7597–7608. [CrossRef]
37. Afandy, M.A.; Sawali, F.D.I. Model Isotherm Multi Parameter Pada Proses Adsorpsi Cr (VI) Menggunakan Arang Kayu Teraktivasi Asam. *War. Akab* **2025**, *49*, 48–54. [CrossRef]
38. Shahrabadi, A.; Daghbandan, A.; Arabiyoun, M. Experimental Investigation of the Adsorption Process of the Surfactant-Nanoparticle Combination onto the Carbonate Reservoir Rock Surface in the Enhanced Oil Recovery (EOR) Process. *Chem. Thermodyn. Therm. Anal.* **2022**, *6*, 100036. [CrossRef]

39. Alomar, T.; Hameed, B.H.; Al-Ghouti, M.A.; Almomani, F.A.; Han, D.S. A Review on Recent Developments and Future Prospects in the Treatment of Oily Petroleum Refinery Wastewater by Adsorption. *J. Water Process Eng.* **2024**, *64*, 105616. [CrossRef]
40. Talebian, S.H.; Sagir, M. Adsorption Behavior of In-House Developed CO_2-Philic Anionic Surfactants. *Sci. Rep.* **2024**, *14*, 24500. [CrossRef]
41. dos Borges, V.F.S.; Monteiro, M.K.S.; Filho, E.D.D.S.; Silva, D.C.D.; Fonseca, J.L.C.; Neto, A.O.W.; Braga, T.P. Study of the Adsorption of Anionic Surfactants on Carbonate Rocks: Characterizations, Experimental Design, and Parameter Implementation. *Coatings* **2024**, *14*, 856. [CrossRef]
42. Kurniawan, S.B.; Imron, M.F.; Sługocki, Ł.; Nowakowski, K.; Ahmad, A.; Najiya, D.; Abdullah, S.R.S.; Othman, A.R.; Purwanti, I.F.; Hasan, H.A. Assessing the Effect of Multiple Variables on the Production of Bioflocculant by Serratia Marcescens: Flocculating Activity, Kinetics, Toxicity, and Flocculation Mechanism. *Sci. Total Environ.* **2022**, *836*, 155564. [CrossRef] [PubMed]
43. Imron, M.F.; Ananta, A.R.; Ramadhani, I.S.; Kurniawan, S.B.; Abdullah, S.R.S. Potential of Lemna Minor for Removal of Methylene Blue in Aqueous Solution: Kinetics, Adsorption Mechanism, and Degradation Pathway. *Environ. Technol. Innov.* **2021**, *24*, 101921. [CrossRef]
44. Ezzati, R.; Azizi, M.; Ezzati, S. A Theoretical Approach for Evaluating the Contributions of Pseudo-First-Order and Pseudo-Second-Order Kinetics Models in the Langmuir Rate Equation. *Vacuum* **2024**, *222*, 113018. [CrossRef]
45. González-Fernández, L.A.; Aguirre-Contreras, S.; Medellín-Castillo, N.A.; Sánchez-Polo, M.; Navarro-Frómeta, A.E.; Leyva-Ramos, R.; Vilasó-Cadre, J.E.; Ocampo-Pérez, R. Mathematical Modelling of Kinetic and Breakthrough Curves for Cd(II) Adsorption onto Sargassum Biomass Using the Diffusion—Permeation Model. *J. Water Process Eng.* **2025**, *77*, 108473. [CrossRef]
46. Rahmanian, O.; Dinari, M.; Mohammadi, N.; Aliakbarian, L. Synthesis, Characterization, and Adsorption Performance of Naphthalene-Based Covalent Organic Polymer for High-Efficiency Methylene Blue Removal. *Sci. Rep.* **2024**, *14*, 29029 . [CrossRef] [PubMed]
47. Bakalis, E.; Zerbetto, F. Adsorption Kinetics: Classical, Fractal, or Fractional? *Langmuir* **2025**, *41*, 19834–19844. [CrossRef] [PubMed]
48. Montazeri, M.; Fazelabdolabadi, B.; Shahrabadi, A.; Nouralishahi, A.; HallajiSani, A.; Moosavian, S.M.A. An Experimental Investigation of Smart-Water Wettability Alteration in Carbonate Rocks–Oil Recovery and Temperature Effects. *Energy Sources Part A Recovery Util. Environ. Eff.* **2024**, *46*, 7798–7810. [CrossRef]
49. Nwabanne, J.T.; Iheanacho, O.C.; Obi, C.C.; Onu, C.E. Linear and Nonlinear Kinetics Analysis and Adsorption Characteristics of Packed Bed Column for Phenol Removal Using Rice Husk-Activated Carbon. *Appl. Water Sci.* **2022**, *12*, 91. [CrossRef]
50. Serafin, J.; Dziejarski, B. Application of Isotherms Models and Error Functions in Activated Carbon CO_2 Sorption Processes. *Microporous Mesoporous Mater.* **2023**, *354*, 112513. [CrossRef]
51. Kisiela-Czajka, A.M.; Dziejarski, B. Linear and Non-Linear Regression Analysis for the Adsorption Kinetics of SO2 in a Fixed Carbon Bed Reactor—A Case Study. *Energies* **2022**, *15*, 633. [CrossRef]
52. Zulfikar, M.A.; Mariske, E.D.; Djajanti, S.D. Adsorption of Lignosulfonate Compounds Using Powdered Eggshell. *Songklanakarin J. Sci. Technol.* **2012**, *34*, 309–316.
53. Wu, Y.; Chen, W.; Dai, C.; Huang, Y.; Li, H.; Zhao, M.; He, L.; Jiao, B. Reducing Surfactant Adsorption on Rock by Silica Nanoparticles for Enhanced Oil Recovery. *J. Pet. Sci. Eng.* **2017**, *153*, 283–287. [CrossRef]
54. Zhao, M.; Cheng, Y.; Wu, Y.; Dai, C.; Gao, M.; Yan, R.; Guo, X. Enhanced Oil Recovery Mechanism by Surfactant-Silica Nanoparticles Imbibition in Ultra-Low Permeability Reservoirs. *J. Mol. Liq.* **2022**, *348*, 118010. [CrossRef]
55. Supriyadi, D.; Darmansyah; Sari, R.P.; Farhani, A.C. Application of Non-Linear Kinetic and Isotherm Model for Investigation of Cod Removal from Tapioca Liquid Waste Onto Modified Lampung Natural Zeolite. *Sci. Technol. Indones.* **2021**, *6*, 218–227. [CrossRef]